OPEN ACCESS Freely available online

ISSN 2737-5323
Volume 5, Issue 2
https://afm.iikii.com.sg
Applied Functional Materials

Article

Design and Fabrication of Humidity Sensors Based on Ceramic Thin Films

Wei-Cheng Huang [1], Yun-Cheng Li [1], Sutatch Ratanaphan [2], Lung-Ming Fu [3], and Chia-Yen Lee [1,*]

[1] Department of Materials Engineering, National Pingtung University of Science and Technology, Pingtung 912, Taiwan; kevin6d06@gmail.com (W.-C. H.), cli521314@gmail.com (Y.-C. L.)

[2] Department of Tool and Materials Engineering, King Mongkut's University of Technology Thonburi, Bangkok 10140, Thailand; sutatch@gmail.com

[3] Department of Engineering Science, National Cheng Kung University, Tainan 701, Taiwan; loudyfu@mail.ncku.edu.tw

* Correspondence: leecy@mail.npust.edu.tw

Received: Jun 04, 2025; **Revised:** Jun 20, 2025; **Accepted:** Jun 25, 2025; **Published:** Jun 30, 2025

Abstract: This research utilizes Micro-Electro-Mechanical Systems (MEMS) technology to develop a resistance-based humidity sensor fabricated on an aluminum oxide (Al_2O_3) substrate. Microfabrication techniques are first employed to pattern the temperature and humidity sensing electrodes on the Al_2O_3 substrate. Electron Beam Evaporation (EBE), followed by a lift-off procedure, is then used to pattern platinum (Pt) and chromium (Cr) electrodes for temperature and humidity sensing, respectively. Finally, radio frequency (RF) sputtering is performed to deposit thin layers of titanium dioxide (TiO_2) and tungsten trioxide (WO_3) on the electrodes as sensing layers. The working temperature and humidity are measured concurrently by monitoring the resistance signals of the device using LabVIEW software. The effects of the sputtering and annealing times on the structures of the two ceramic films are explored. In addition, the corresponding changes in the temperature and humidity sensing performance are evaluated and compared. The results show that the TiO_2 film has a better moisture expulsion capability than the WO_3 film. Consequently, the sensor incorporating the TiO_2 film shows a superior sensitivity and faster response time. The maximum sensitivity is observed in the sample annealed at 450°C for 4 h owing to the formation of optimally-sized pores that enhance moisture absorption and removal.

Keywords: Humidity sensor, Micro-Electro-Mechanical systems, Titanium dioxide, Tungsten trioxide

1. Introduction

Humidity is an essential concern in many industries and environments due to its impact on human health, product quality, and material durability. Physically, the optimal relative humidity range for the human body is 40 to 60%. Excessive humidity can exacerbate respiratory issues and increase susceptibility to allergies due to the proliferation of dust mites and mold. Furthermore, environments with excessive humidity can encourage mold growth, which may further affect human health. In the industrial and medical domains, environments with inadequate humidity control can lead to the deterioration of products and spoilage of medicine. Thus, effective humidity monitoring and control are essential for improved safety, comfort, and quality.

Humidity-sensing materials can be broadly categorized as ceramics, electrolytes, polymers, and composites. Among them, ceramic humidity sensors provide a particularly sensitive and reliable performance due to their nanometer-sized particles and porous thin-film structures [1]. The relationships between processing condition, microstructure of porous ceramics and humidity sensing properties will be systematically investigated [2]. Ceramics—particularly metal oxides—are distinguished by their numerous advantages, including mechanical robustness, chemical durability, and thermal resilience [3]. Metal oxides such as ZnO, SnO_2, and TiO_2 have been extensively studied for humidity sensing applications due to their high chemical stability, sensitivity, and ease of fabrication [4]. Among the many different materials, titanium dioxide has been extensively studied due to its semiconductor behavior [5]. It has received great attention for application as chemical sensors because of changes in its properties when exposed to different atmospheres. The main sensing mechanism in porous titania corresponds to the adsorption of surrounding water vapors by the oxide surface, which leads to a decrease in the ceramic electrical impedance [6]. Titanium dioxide has different crystalline phases: brookite, anatase and rutile. The electrical variations observed in the humidity measurements in ceramic sensors are originated by the chemical and physical sorptions of water molecules existing in the atmosphere [7]. The impedance changes that a ceramic metal oxide material experiments, when the sensor surface is exposed to a

certain moisture concentration allow their use as humidity sensor [8]. Additionally, the sensitivity of the ceramic sensor is influenced by the porous microstructure and by the surface reactivity with the humidity: so if the sensitivity of these sensors depends on the microstructure, then the fabrication process becomes a strategic tool to improve the sensors response.

At present, humidity sensors need to have not only a high response, short response/recovery time, small humidity hysteresis, and low cost, but also high reliability and stability [9]. However, further research is still necessary to enhance the performance of ceramic sensors, addressing challenges such as the response time, durability, and cost efficiency. The present study aims to meet this need by conducting a detailed investigation of the structural and functional enhancements of two ceramic-based humidity sensors, focusing particularly on optimizing the fabrication and annealing conditions to achieve superior performance in practical applications. The transduction mechanism of resistive humidity sensors involves the changes in conductivity caused by the adsorption of water vapor [10].

The Internet of Things (IoT) and trillion sensor universe have developed remarkably in recent years, bringing about the advanced requirements for fast response, low power consumption and low-cost sensor devices [11]. Among all types of humidity sensors, the resistive-type ones enjoy a promising prospect under the background of the dramatic growth of IoT sensors, which mainly thanks to their simple structures, low price and high compatibility with semiconductor technology.

2. Materials and Methods

2.1. Material Properties

Two ceramic materials were used as sensing layers in the proposed humidity sensors: titanium dioxide (TiO_2) and tungsten trioxide (WO_3). The properties of the two materials are briefly described in the following paragraphs.

Titanium dioxide (TiO_2) is utilized in humidity sensors primarily due to its crystalline structure, which can exist in anatase or rutile forms. The anatase phase, in particular, is favored for humidity sensing owing to its high surface area and superior reactivity. However, in both structures, the titanium ions are coordinated by oxygen in a manner that allows for the adsorption of water molecules, leading to changes in the electrical conductivity and resistivity in response to different humidity levels. The sensitivity of TiO_2 to moisture is enhanced by its semiconducting properties. In particular, when water molecules adsorb onto the surface of TiO_2, they change the concentration of the electron charge carriers, resulting in a measurable change in the electrical properties of the sensing layer.

Tungsten trioxide (WO_3) has a complex crystal structure. Although it may exist in several polymorphic forms, it is most commonly present as monoclinic, triclinic, or cubic phase. Among these three phases, monoclinic WO_3 shows the greatest stability, with a three-dimensional structure consisting of a distorted octahedral coordination of tungsten ions surrounded by oxygen. This structure not only contributes to the semiconducting properties of WO_3 but also allows for the incorporation of water molecules within the lattice, enhancing its sensitivity to humidity changes. Moreover, the ability of WO_3 to undergo phase transitions between its various forms under different ambient conditions further enhances its versatility for humidity sensing applications.

2.2. Sensor Design and Fabrication

The TiO_2 and WO_3 sensors featured a layered structure, integrating a resistance temperature detector (RTD) with a highly sensitive sensing film to enhance the measurement accuracy (Fig. 1) [12]. The sensing principle was based on changes in the resistance or capacitance of the TiO_2 and WO_3 ceramic layers in response to humidity variations. The fabrication process employed conventional microelectromechanical system (MEMS) techniques, including photolithography, metal deposition, and radio frequency (RF) sputtering. The built-in RTD structures provided temperature compensation that ensure the stability and accuracy of the measurement process.

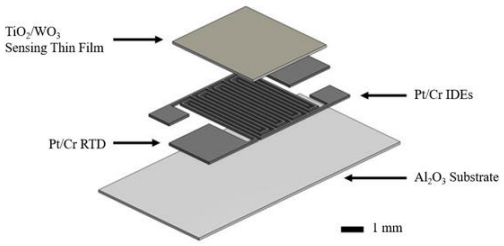

Fig. 1. Schematic of proposed humidity sensors.

Figure 2 illustrates the basic steps of the sensor manufacturing process. First, resistance temperature detector (RTD) and interdigitated electrode (IDE) regions were patterned on alumina substrates using a photolithography process [13]. 35-nm chromium (Cr) adhesion layers and 125-nm platinum (Pt) layers were then evaporated onto the substrate to form the RTD and IDE structures. Ceramic sensing layers (TiO_2 and WO_3) were then deposited by radio frequency sputtering. Finally, the sensor wafers were annealed at an appropriate temperature and duration and then left to cool in the furnace. The annealing process enhanced the sensitivity of the ceramic films by promoting the formation of crystal structures and increasing the porosity, thereby improving the moisture adsorption capacity.

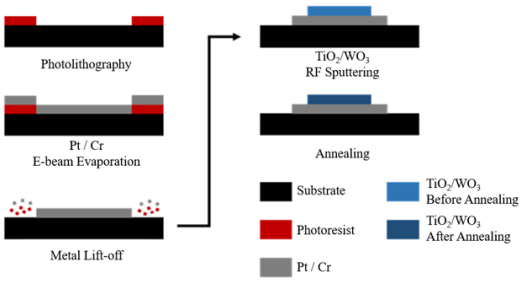

Fig 2. Fabrication workflow of proposed humidity sensors.

3. Results

3.1. Material Tests

The crystal structures of the annealed films were examined using X-ray diffraction (XRD) (D/max-2200/PC, Rikagu, Japan). The surface microstructures were observed using field-emission scanning electron microscopy (FE-SEM; JSM-7600F, JEOL, Japan). The chemical compositions of the films were determined using an energy-dispersive X-ray (EDS) system (Xmax50, Oxford Instruments, Taiwan) installed on the SEM. The RTDs in the sensors were calibrated using a TH-3800 thermo-hygrometer. The humidity sensing performance of the two devices was evaluated in a test chamber using a resistance meter (Fluke 289, CCICO, Taiwan).

3.1.1. X-ray Diffraction (XRD) Analysis Results

Figure 3. (a) shows the XRD patterns of the TiO_2 sensing layers annealed at 450°C for different durations (2, 4, and 6 h). The sample annealed for 4 h shows the highest intensity peaks, indicating that it has the best crystallinity. In humidity sensing applications, the (101) and (104) crystal directions of TiO_2 are more important for the adsorption and removal of water molecules than the peaks in other directions. The (101) orientation, which is typically the most stable orientation, is characteristic of anatase crystals and demonstrates a high capacity for water molecule adsorption. The (104) orientation may be associated with surface defects. A higher crystallinity generally means fewer structural defects, which helps provide more stable electron transport and surface reactions [14]. Therefore, based on the XRD results, compared with the 2-h and 6-h samples, the 4-h sample is expected to provide a superior humidity sensing performance, combining high sensitivity with a shorter response time.

Figure 3. (b) shows the XRD patterns of the WO_3 thin films annealed at 500°C for different durations (1, 2, and 3 h). For all three samples, the patterns contain characteristic (002) and (200) peaks. Stronger (002) and (200) peaks typically indicate enhanced crystallinity, which promotes the formation of oxygen vacancies. This enhances the surface activity and charge transfer capability of the film [15], ultimately leading to better adsorption and increased sensitivity to water vapor. Overall, the XRD patterns suggest that the 2-h sample is likely to provide a slightly better humidity sensing performance than the 1-h or 3-h sample.

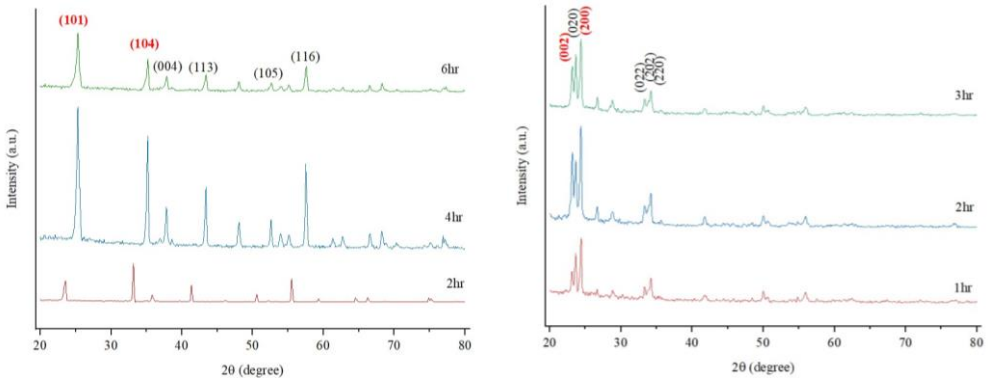

Fig. 3. XRD patterns of (**a**) TiO_2 and (**b**) WO_3 thin films annealed for different durations.

3.1.2. Scanning Electron Microscopy (SEM) Analysis Results

Figure 4. (a)-(d) presents SEM images of the TiO_2 film before and after annealing. As shown, the as-deposited film consists of small, densely packed particles with indistinct grain boundaries, suggesting a high density of grain defects and poor crystallinity. After annealing, the grains become larger and the grain boundaries more distinct, indicating grain growth, the release of internal stress, and an overall improvement in crystallinity. A reduction in surface defects is also observed, which enhances the stability of water vapor adsorption and desorption on the surface. Overall, the increased grain size and clearer grain boundaries of the annealed structure contribute to improved crystallinity, leading to superior carrier mobility and more stable electron transport.

The SEM images in Fig. 4. (e)-(h) show that after annealing, the particle size of the WO_3 film increased, and the crystal gaps expanded significantly, thereby facilitating the efficient diffusion and adsorption of water molecules. The annealed WO_3 layer exhibits a more crystalline structure. The improved crystallinity increases the concentration of oxygen vacancies, further influencing the reaction mechanism between WO_3 and the water molecules and amplifying the resistance change. Consequently, both the sensitivity and the stability of the WO_3 sensing layer are improved.

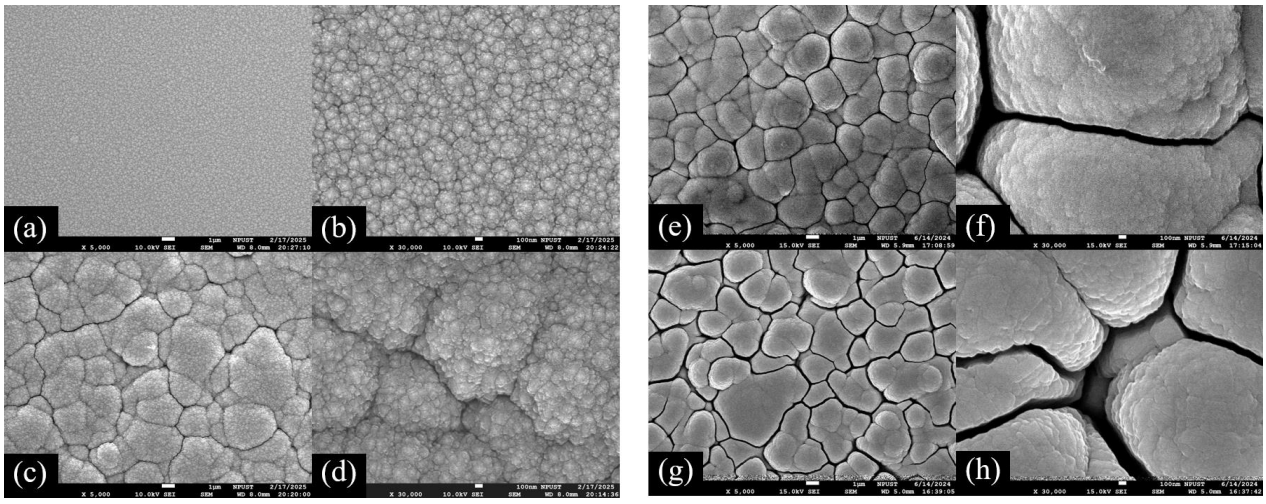

Fig. 4. SEM surface microstructures of TiO_2 thin films: (**a**) before annealing (5000× magnification), (**b**) before annealing (30000× magnification), (**c**) after annealing (5000× magnification), and (**d**) after annealing (30000× magnification). SEM surface microstructures of WO_3 thin films: (**e**) before annealing (5000× magnification), (**f**) before annealing (30000× magnification), (**g**) after annealing (5000× magnification), and (**h**) after annealing (30000× magnification).

3.1.3. Energy-dispersive X-ray (EDS) System Analysis Results

Figure 5. (a) shows the EDS analysis results for the annealed TiO_2 sensing layer. The layer consists mainly of titanium (Ti) and oxygen (O) (Table 1). The EDS spectrum reveals a stronger oxygen signal, which can be attributed to oxidation during the high-temperature annealing process. This process facilitates the adsorption and diffusion of additional oxygen from the environment into the material, resulting in a higher oxygen ratio.

Figure 5. (b) and Table 2 show that the annealed WO_3 sensing layer is mainly composed of tungsten (W) and oxygen (O). As for the TiO_2 film, the EDS spectrum shows a strong oxygen signal, which can be attributed to oxidation during the high-temperature annealing process.

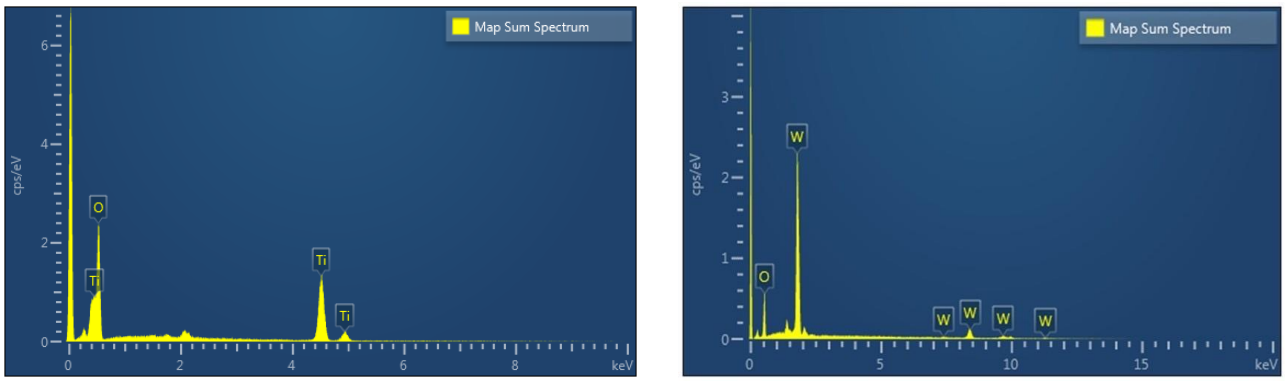

(a) **(b)**

Fig. 5. EDS analysis results for annealed (**a**) TiO_2 and (**b**) WO_3 sensing layer.

Table 1. Element composition of annealed TiO_2 sensing layer.

Element	Wt.%	At.%
O	46.65	72.36
Ti	53.35	27.64
Total	100.00	100.00

Table 2. Element composition of annealed WO_3 sensing layer.

Element	Wt.%	At.%
O	24.50	78.85
W	75.50	21.15
Total	100.00	100.00

3.2. Experimental Results

During the testing process, both the temperature and the humidity affect the resistance of the sensing layer. Therefore, a temperature dry tester was first used to determine the temperature. The resistance values of the temperature sensor and humidity sensor were then tested separately. The resistance values were converted to voltage values using the voltage divider method. Finally, both measurements were integrated to obtain the current temperature and humidity.

3.2.1. Temperature Test Result

In temperature sensing, it is crucial to ensure that the humidity does not significantly influence the resistance variation. To verify this for the present sensors, temperature measurements were conducted under two distinct humidity conditions: 40% RH and 90% RH. The results presented in Fig. 6 confirm that the humidity had only a negligible effect on the resistance of the temperature sensor.

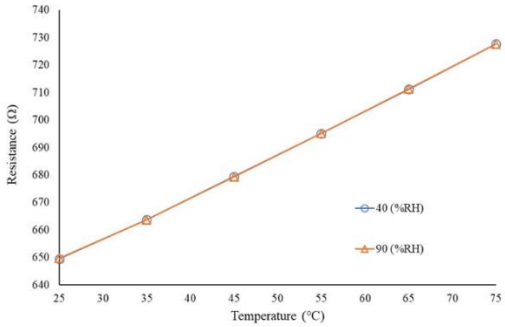

Fig. 6. Sensitivity of temperature sensor under different humidity conditions.

3.2.2. Humidity Test Results

Figure 7. (a) shows the relationship between the resistance change and the relative humidity (%RH) for the TiO_2 sensor at different working temperatures (25°C, 50°C, and 75°C). At all three temperatures, the resistance decreases exponentially with an increasing humidity. This trend is mainly attributed to the physical and chemical adsorption of water molecules on the sensing surface, which leads to a higher carrier concentration and a lower resistance. At a given humidity, the resistance reduces with an increasing temperature. This suggests that a higher temperature accelerates the adsorption-desorption dynamic equilibrium of the water molecules, making the conductive properties of the material more stable. All three curves show high correlation coefficients (R^2). In other words, the TiO_2 sensor has good sensitivity and response characteristics over the considered temperature range. Overall, the results indicate that the sensor provides an effective sensing performance, particularly in the low-humidity range and room temperature conditions.

Figure 7. (b) shows the variation of the resistance with the relative humidity (%RH) for the WO_3 sensor at working temperatures of 25°C, 50°C, and 75°C. As for the TiO_2 sensor, the resistance reduces with increasing humidity, albeit more slowly. The lower resistance arises from a greater adsorption of water molecules on the surface, which promotes charge transfer and improves the conductivity. In the low-humidity range (40-60% RH), the resistance change is relatively low. However, in the high-humidity range (70-90% RH), the resistance drop is more apparent. For a given humidity, the resistance decreases with increasing temperature since the higher temperature accelerates the adsorption and desorption of the water molecules, thereby improving the charge transfer ability of the WO_3 layer. At room temperature, the correlation coefficient has a value of $R^2 = 0.9846$, which indicates a strong correlation between the humidity and the sensor resistance. At the highest temperature of 75°C, the correlation coefficient drops to $R^2 = 0.8824$. This finding suggests that higher temperatures may cause more dramatic changes in the dynamics of the water molecules or changes in the concentration of the oxygen vacancies inside the sensing layer, which subsequently affect the conduction mechanism. Overall, however, the results indicate that the WO_3 sensor also provides a feasible solution for humidity sensing, particularly in the low-humidity range and room temperature conditions.

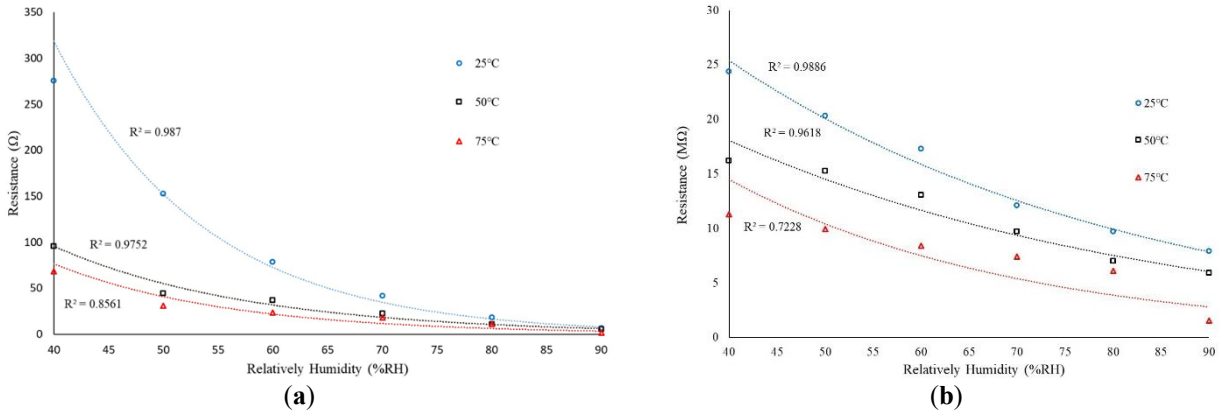

Fig. 7. Sensitivity of (**a**) TiO_2 and (**b**) WO_3 humidity sensor at different working temperatures.

3.3. Response/Recovery Time Tests

To evaluate the response time of the humidity sensor, the sensor was first isolated in a chamber with a normal concentration of humidity (approximate 45% RH). The humidity concentration was then increased rapidly to 100% RH, and the time required

for the sensor signal to reach 90% of its final equilibrium value was recorded. The corresponding results are presented in Fig. 8. (a).

For TiO_2 humidity sensors, the process depends on how quickly water molecules desorb from the material's surface. Due to the porosity of TiO_2, the recovery time will be fast. Fig. 8. (b) shows the result of the experiment. When the humidity drops from 95% RH to 40% RH, the sensor can recover within 2 seconds.

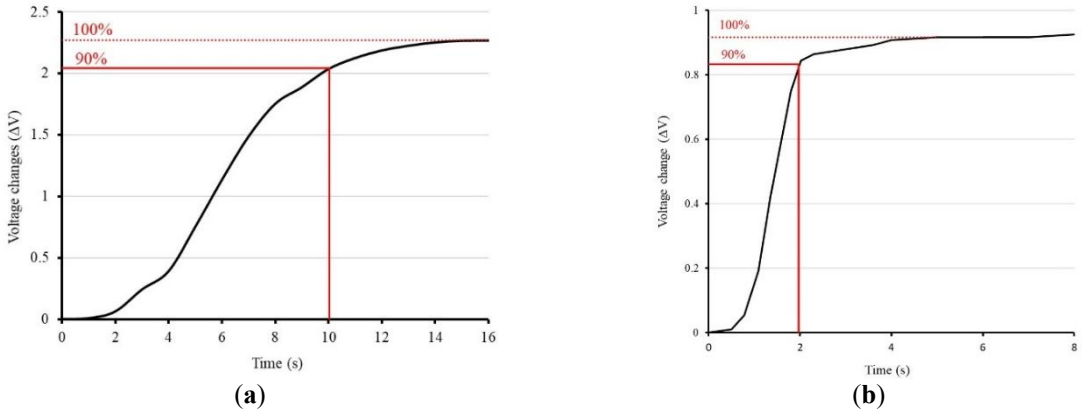

Fig. 8. (**a**) Response time and (**b**) Recovery time of TiO_2 humidity sensor.

3.4. Integration Test

Figure 9. (a) shows the voltage changes of TiO_2 sensor at 25°C, 50°C and 75°C for relative humidity (40%–90%). The figures include the actual mea-surement data (measuring line) and the integrated curve (integrated line) calculated by integrating the temperature-compensated humidity sensing formula. The purpose of this study is to use temperature-compensated humidity sensors. The temperature factor is written into the formula through a mathematical model and the sensor is compensated to improve the accuracy and stability of the sensor under different environmental conditions.

The result of WO_3 sensor in Fig. 9. (b) also shows a similar trend. The voltage gradually decreases with the increase of humidity. The voltage also shows a downward trend at high temperature, indicating that its humidity-sensitive properties are also affected by temperature. Incorporating temperature compensation into the formula not only improves the accuracy of the sensors, but also makes it more stable in actual applications.

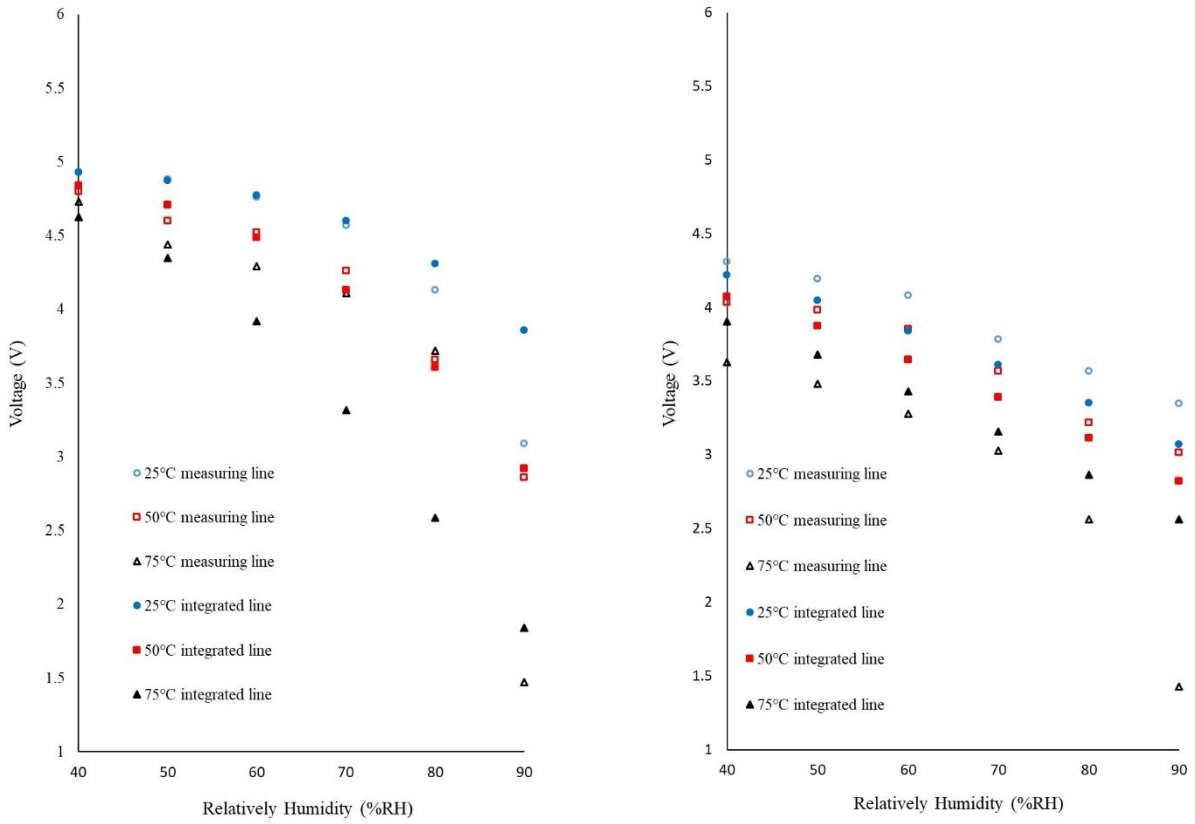

Fig. 9. Integration of (**a**) TiO_2 and (**b**) WO_3 humidity sensor at different working temperatures.

Figure 10. shows the sensor data processing program written in Lab-VIEW. The purpose is to bring the real-time measured voltage value into the formula written in LabVIEW and obtain the temperature and humidity of the current environment. Programming is divided into: switch control logic, temperature data acquisition and calculation, and temperature and humidity integration formula calculation and result display. First, the Boolean switch element on the left is used for logic control. When the switch is "True", the entire process is started. Then the system reads the voltage signal of the sensor in real time through the DAQ device, corresponding to the two sets of inputs: temperature (DAQ Temperature data) and humidity (DAQ Humidity data). For the temperature part, the voltage measured by the RTD is brought into the linear regression model of the temperature in the program. In the humidity calculation process, the calculated temperature will be used as one of the input parameters and substituted into the preconstructed temperature and humidity integration formula to obtain the current humidity. Wherein, x is the voltage sensed by the interdigitated electrode, y is the calculated temperature value, and z is the required relative humidity. The final calculation results will be output to the numerical display components on the right, labeled as tem-perature and humidity.

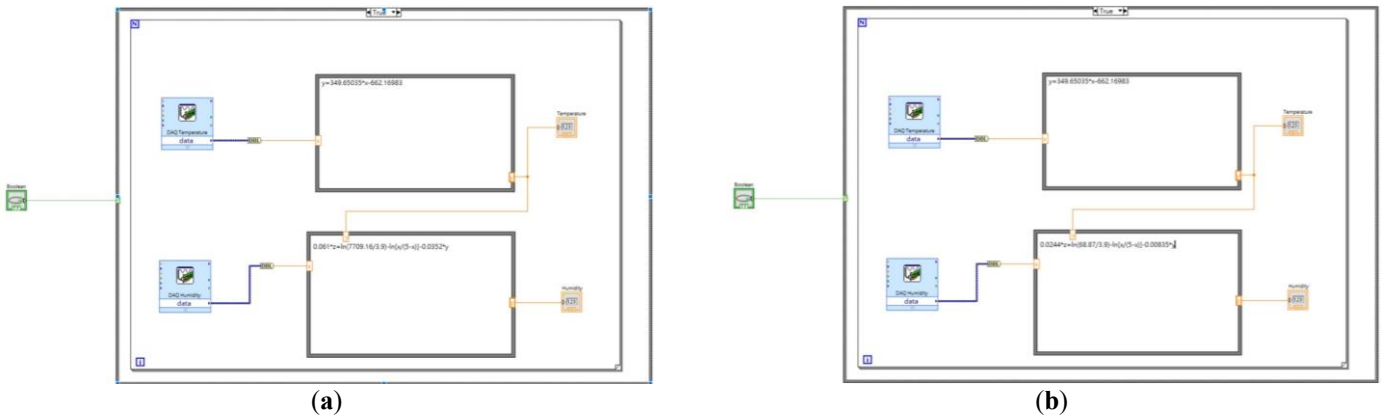

Fig. 10. Block diagram of LabVIEW for (**a**) TiO_2 and (**b**) WO_3.

After LabVIEW calculation, the temperature and humidity of the environ-ment can be obtained. Ideally, the computational quality should be the same as that of a normal sensor. Figure 11. shows that the correlation coefficients of the two materials at three different temperatures were taken with the ideal values and then averaged. The average correlation coefficient between the calculated value and the measured value of TiO_2 is 0.9934, while the correlation coefficient between the calculated value and the measured value of WO_3 is only 0.9636. TiO_2 not only has a higher average correlation coefficient, but the distributions of the three temperatures are also closer to the ideal values. Therefore, it can be concluded that TiO_2 is more suitable as a sensing layer material than WO_3. The high correlation coefficients of the two materials indicate that both materials have potential as humidity sensing layers.

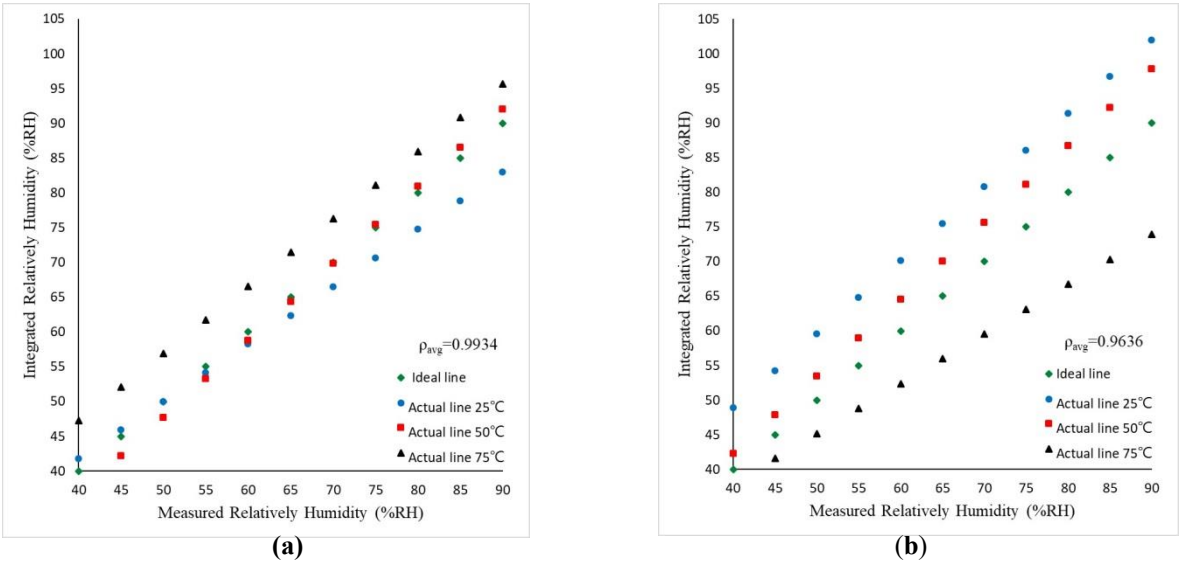

Fig. 11. Comparison of measured and calculated values of (**a**) TiO_2 and (**b**) WO_3.

4. Conclusions

This study used microelectromechanical system (MEMS) process technology to fabricate humidity sensors incorporating titanium dioxide (TiO_2) and tungsten trioxide (WO_3) ceramic sensing layers. The performance of the two sensors was systematically explored under various temperature and humidity conditions. For both sensors, the resistance reduced with an increasing temperature owing to a more rapid adsorption-desorption dynamic equilibrium of the water molecules, which caused the conductive properties of the material to become more stable.

The results showed that both sensors exhibited a measurable change in resistance when exposed to different levels of humidity in the range of 40–90% RH. The sensors used in the experiment all use interdigitated electrodes. From the aforementioned research, it is known that because there are more contact points, the sensitivity of resistance signal measurement can be improved, and the experimental results also verify this statement. However, of the two sensors, the sensor with a TiO_2 ceramic layer exhibited a better sensitivity owing to its higher moisture adsorption ability. The porous nature of ceramics makes it easier to absorb and dehumidify moisture. The superior sensing performance of the TiO_2 device is particularly evident when the sensing layer is annealed at 450°C for 4 h, as the elevated temperature reduces the number and severity of surface defects, as evidenced by the significantly increased overall peak intensity in the XRD pattern, indicating better crystallinity, thereby enhancing the stability of water vapor adsorption and desorption on the sensing surface. Observation of the surface structure under SEM shows that the grains are significantly enlarged, increasing the contact area with water vapor. The WO_3 sensor exhibited a good sensing performance under low-humidity conditions. However, the sensitivity reduced at higher humidity due to dramatic changes in the dynamics of the water molecules and changes in the concentration of the oxygen vacancies inside the sensing layer.

In summary, the sensors developed in this study demonstrate a stable operation with good sensitivity under various environmental conditions. The TiO_2 sensor, in particular, exhibits a significant change in resistance in response to changing humidity conditions. The findings presented in this study have significant practical implications for a wide range of applications in environmental monitoring, industrial processes, and emerging technologies where accurate and reliable humidity sensing is essential.

Author Contributions: conceptualization, L.M. Fu and C.Y. Lee; methodology, W.C. Huang, Y.C. Li and C.Y. Lee; software, W.C. Huang and Y.C. Li; validation, W.C. Huang, Y.C. Li and S. Ratanaphan; investigation, W.C. Huang, Y.C. Li and L.M. Fu; resources, S. Ratanaphan, L.M. Fu and C.Y. Lee; data curation, W.C. Huang and Y.C. Li; writing—original draft preparation, W.C. Huang and Y.C. Li.; writing—review and editing, S. Ratanaphan and L.M. Fu; supervision, C.Y. Lee. All authors have read and agreed to the published version of the manuscript.

Funding: This research did not receive external funding.

Data Availability Statement: The data of this study are available from the corresponding author upon reasonable request.

Conflicts of Interest: The authors declare no conflict of interest.

References

1. Kassas, A.; Zahwa, I.; Hussein, B.; Bernard, J.; Lelièvre, C.; Mouyane, M.; Noudem, J.; Houivet, D. Enhanced humidity sensing performance of LiF-doped $MgTiO_3$ ceramics via spark plasma sintering. *Heliyon*. **2024**, *10*, e33999. https://doi.org/10.1016/j.heliyon.2024.e33999
2. Chou, K. S.; Lee, T. K.; Liu, F. J. Sensing mechanism of a porous ceramic as humidity sensor. *Sensors and Actuators B*. **1999**, *56*, 106–111. https://doi.org/10.1016/S0925-4005(99)00187-2
3. Thanamoon, N.; Thongyong, N.; Sreejivungsa, K.; Chanlek, N.; Jarernboon, W.; Thongbai, P. Outstanding dielectric permittivity and humidity sensitivity in (Y/Sb) co-doped TiO_2 ceramics with rapid response/recovery time. *Sensors and Actuators: B. Chemical*. **2024**, *419*, 136372. https://doi.org/10.1016/j.snb.2024.136372
4. Choudapur, V.H.; V, J. A.; Tudorache, F.; Ayachit, N.H.; Shaikh, S. F.; Ubaidullah, M. Structural, Optical and Humidity Sensing performance of Lanthanum doped $CoCr_2O_4$ nano-ceramics for Sensor Applications. *Ceramics International*. **2024**, *50*, 44056–44067. https://doi.org/10.1016/j.ceramint.2024.08.255
5. Rochaa, K.O.; Zanetti, S.M. Structural and properties of nanocrystalline WO_3/TiO_2-based humidity sensors elements prepared by high energy activation. *Sensors and Actuators B*. **2011**, *157*, 654–661. https://doi.org/10.1016/j.snb.2011.05.048
6. Wang, X.; Li, J. H.; Li, Y. L.; Liu, L. J.; Guan, W. M. Emulsion-templated fully three-dimensional interconnected porous titania ceramics with excellent humidity sensing properties. *Sensors and Actuators B*. **2016**, *237*, 894–898. https://doi.org/10.1016/j.snb.2016.07.014
7. Faia, P.M.; Ferreira, A.J.; Furtado, C.S. Establishing and interpreting an electrical circuit representing a TiO_2–WO_3 series of humidity thick film sensors. *Sensors and Actuators B*. **2009**, *140*, 128–133. https://doi.org/10.1016/j.snb.2009.04.016
8. Faiaa, P. M.; Libardib, J.; Louro, C. S. Effect of V_2O_5 doping on p- to n-conduction type transition of TiO_2:WO_3 composite humidity sensors. *Sensors and Actuators B*. **2016**, *222*, 952–964. https://doi.org/10.1016/j.snb.2015.09.039
9. Li, P.; Yang, F. Preparation and performance of TiO_2/ZnO humidity sensor based on TiO_2. *Materials Science and Engineering B*. **2023**, *298*, 116902. https://doi.org/10.1016/j.mseb.2023.116902
10. Lee, C. Y.; Lee, G. B. Humidity Sensors: A Review. *Sensor Letters*. **2005**, *3*, 1–14. https://doi.org/10.1166/sl.2005.001
11. Zhang, C.; Zhang, Y.; Cao, K.; Guo, Z.; Han, Y.; Hu, W.; Wu, Y.; She, Y.; He, Y. Ultrasensitive and reversible room-temperature resistive humidity sensor based on layered two-dimensional titanium carbide. *Ceramics International*. **2021**, *47*, 6463–6469. https://doi.org/10.1016/j.ceramint.2020.10.229
12. Lina, X.; Zhanga, C.; Yanga, S.; Guoc, W.; Zhang, Y.; Yang, Z.; Ding, G. The impact of thermal annealing on the temperature dependent resistance behavior of Pt thin films sputtered on Si and Al_2O_3 substrates. *Thin Solid Films*. **2019**, *685*, 372–378. https://doi.org/10.1016/j.tsf.2019.06.036
13. Omran, H.; Salama, K. N. Design and fabrication of capacitive interdigitated electrodes for smart gas sensors. *3rd IEEE International Conference on Smart Instrumentation Measurement and Applications (ICSIMA)*, Kuala Lumpur, Malaysia, November 24-25, 2015. https://doi.org/10.1109/ICSIMA.2015.7559021
14. Zhu, Z.; Long, Y.; Xue, X.; Yin, Y.; Zhu, B.; Xu, B. Phase-transition kinetics of calcium-doped TiO_2: A high-temperature XRD study. *Ceramics International*. **2022**, *48*, 25056–25063. https://doi.org/10.1016/j.ceramint.2022.05.160
15. Brüger, A.; Fafilek, G.; Neumann-Spallart, M. Identification of different WO_3 modifications in thin films for photocatalytic applications by peak shape analysis in high temperature XRD diffractometry. *Journal of Photochemistry & Photobiology, A: Chemistry*. **2024**, *457*, 115879. https://doi.org/10.1016/j.jphotochem.2024.115879